Petroleum Science 22 (2025) 2262–2273

Contents lists available at ScienceDirect

Petroleum Science

journal homepage: www.keaipublishing.com/en/journals/petroleum-science

Original Paper

The fractal characteristics of the pore throat structure of tight sandstone and its influence on oil content: A case study of the Chang 7 Member of the Ordos Basin, China

Peng Li [a, b, c, *], Bao-Jian Shen [a, b, c], Ya-Li Liu [a, b, c], He Bi [d, **], Zhong-Bao Liu [a, b, c], Rui-Kang Bian [a, b, c], Peng-Wei Wang [a, b, c], Pei Li [a, b, c]

[a] State Key Laboratory of Shale Oil and Gas Enrichment Mechanisms and Efficient Development, Beijing, 102206, China
[b] Key Laboratory of Shale Oil/Gas Exploration and Production Technology, SINOPEC, Beijing, 102206, China
[c] Petroleum Exploration and Production Research Institute, SINOPEC, Beijing, 102206, China
[d] Research Institute of Petroleum Exploration and Development, PetroChina, Beijing, 100083, China

ARTICLE INFO

Article history:
Received 27 March 2024
Received in revised form
20 September 2024
Accepted 13 March 2025
Available online 15 March 2025

Edited by Jie Hao

Keywords:
Tight sandstone
Pore throat structure
Fractal
Oil content

ABSTRACT

Tight oil is the most viable target for unconventional oil and gas exploration, but the complexity of micro-/nanopore throat systems significantly affects the oil content of reservoirs. To investigate the causes of heterogeneity in oil-bearing reservoirs, a high-pressure mercury injection experiment combined with fractal theory was conducted to analyze the micro pore throat structure characteristics of the tight sandstone of Chang 7 Member reservoirs in the Ordos Basin. The factors controlling the variations in oil content among tight sandstone samples were identified based on mineral composition characteristics. The results indicate that the pore throat radius distribution is mainly unimodal an bimodal. In oil-bearing samples, the pore throat distributions align well with the corresponding permeability contribution curves, while in oil-free samples, there is a clear deviation from these curves. Mesopore throats exert the greatest influence on seepage capacity. Differences in fractal characteristics are primarily reflected in D1 values, with oil-free samples exhibiting D1 values close to 3, indicating an extremely nonuniform pore throat structure at this scale. The content of quartz, plagioclase, and chlorite is significantly higher in oil-bearing samples than in oil-free samples, whereas calcite content is lower in oil-bearing samples. There is a positive correlation between the contents of quartz, plagioclase, and chlorite with D1; their increased presence contributes to a more favorable pore throat structure. Conversely, the calcite contents show an inverse relationship with D1. Cementation increases the complexity of pore throat structures, while multiple diagenetic processes simultaneously control these characteristics, leading to variations in oil content.

1. Introduction

Given the surging global demand for oil and gas resources, unconventional oil and gas have become pivotal in the field of oil exploration and development (Wang et al., 2016a; Griffin et al., 2022; Jia et al., 2023). As a significant unconventional resource, tight oil has garnered considerable attention from researchers in the petroleum industry (Jia, 2017; Velasco et al., 2018). Tight oil refers to hydrocarbons that are accumulated in adsorbed and free states within reservoir rocks, such as tight sandstone and tight carbonate formations adjacent to source rocks, without undergoing extensive long-distance migration (Jia et al., 2012). Currently, commercial exploitation of tight oil has been successfully achieved in various formations, including the Bakken, Eagle Ford, and Wolfcamp in the United States (Wachtmeister et al., 2017; Male and Duncan, 2022; Ramiro-Ramirez et al., 2024). Significant progress has also been made toward large-scale industrial development in basins such as the Sichuan Basin and Ordos Basin in China (Yang et al., 2017; Li et al., 2019b).

* Corresponding author.
** Corresponding author.
E-mail addresses: lipeng2017.syky@sinopec.com (P. Li), gloria_hebi@126.com (H. Bi).

https://doi.org/10.1016/j.petsci.2025.03.016

The hydrocarbon accumulation and distribution characteristics of tight reservoirs differ significantly from those of conventional sandstone reservoirs (Loucks et al., 2009; Jia, 2017; Li et al., 2022b). The micro-to nanopore throat network system, which is widely distributed in tight reservoirs, is a key factor controlling the accumulation and distribution of tight oil and gas (Lai et al., 2018; Ghanbarian et al., 2019; Jiu et al., 2021; Yang et al., 2023). Compared to the millimeter-to micron-scale pore-throat network system in conventional sandstone, the micro-to nanometer-scale pore-throat network system in tight reservoirs exhibits a complex structure, smaller pore sizes, diverse connectivity, and significant heterogeneity (Nelson, 2009; Xi et al., 2019; Gong and Liu, 2020; Li et al., 2020). Consequently, the mechanisms governing oil and gas charging, migration, and accumulation differ from those observed in conventional large-pore systems (Jia, 2017). This complexity also results in significant heterogeneity in oil content, which serves as a fundamental criterion for evaluating reservoir effectiveness (Jia et al., 2012; Zou et al., 2019; Cao et al., 2021). Exploration and development practices have demonstrated that oil occurrence and distribution within tight sandstone reservoirs exhibit pronounced complexity and heterogeneity at both the core scale and reservoir scale (Li et al., 2019b; Li et al., 2023). These variations lead to noticeable differences in oil content enrichment across different parts of the same tight sandstone reservoir. Such phenomena have become important factors limiting exploration efforts for tight oil and gas reserves. Therefore, it is crucial to enhance research on oil content in tight reservoirs while elucidating the reasons behind variations in oil content within these types of reservoirs (Wang and Philp, 2019; Zou et al., 2019).

Due to the intricate pore structure of tight reservoirs, traditional Euclidean geometry often struggles to accurately describe their heterogeneity. Fractal theory, however, is well-suited for quantifying the complexity and heterogeneity of pore structures and has been widely applied in studying pore throat structures (Mandelbrot et al., 1984; Pfeifer, 1984; Schlueter et al., 1997; Li et al., 2017). The fractal dimension, derived from fractal theory, serves as an ideal parameter for comprehensively describing the regularity and combination characteristics of micro pore throats in reservoir rocks (Anovitz et al., 2013; Wang et al., 2016b; Li et al., 2019a; Zhu et al., 2019). This approach reflects the degree of micro-heterogeneity in reservoir pore throat structures and provides an effective means to quantitatively characterize the size distribution, heterogeneity, and complexity of pores (Giri et al., 2012; Ji et al., 2016; Feng et al., 2020; Zuo et al., 2024).

To identify the causes of oil content heterogeneity, this study utilizes high-pressure mercury injection experiments to analyze the micro pore throat structure characteristics of the tight reservoirs of Chang 7 Member. Additionally, the fractal dimensions of the pore throats in rock samples of different scales are calculated using fractal theory to examine their relationships with parameters characterizing reservoir pore throat structures. By systematically comparing the micro pore throat structure and fractal dimension characteristics between samples with high oil contents and those with low oil contents, while considering mineral composition traits, this research discusses the main factors influencing oil content in tight sandstone reservoirs. These findings provide valuable insights for evaluating the effectiveness of tight reservoirs.

2. Geological setting

The Ordos Basin, situated in central China, is the second largest sedimentary basin in the country, covering a total area of 37×10^4 km^2 (Liu et al., 2013). Its current tectonic pattern has been shaped by both the Yanshan and Himalayan movements. To date, four sets of oil-bearing layers have been discovered in this basin—namely, the Ordovician, Permian, Triassic and Jurassic formations—which boast abundant oil and gas resources (Liu et al., 2009; Feng et al., 2021). Among these formations, the Triassic Yanchang Formation and the Jurassic Yan'an Formation serve as the primary reservoirs for oil. The Ordos Basin can be divided into 6 s-order structural units based on its present structural morphology (Liu et al., 2015). The study area of Xin'anbian is located west of the Yishan slope, encompassing Wuqi County and Dingbian County in Shanxi Province (Fig. 1). Xin'anbian lies in the central-western part of the Ordos Basin, where black shale and sandstone were interbedded during deposition in the period of Chang 7 Member. The tight oil reservoir of Chang 7 Member primarily consists of fine-grained sandstone characterized by poor sorting, high clay content, complex mineral composition, and strong compaction features (Liu et al., 2022; Ma et al., 2022).

Through extensive on-site core observations within our study area, it has been observed that many wells exhibit alternating intervals of oil-bearing and oil-free sections. For instance, consider Well A's sandstone section from 2138 to 2144.04 m depth and Well B's sandstone section from 2193.92 to 2208.22 m depth; these core sections display interstratification between oil-bearing and oil-free sandstones throughout their entirety (Fig. 2). Furthermore, the entire sandstone section exhibits significant heterogeneity regarding its potential for bearing oil: cores with substantial amounts of oil are predominantly brown, while those without any traces of oil appear grey or white.

3. Materials and method

A total of 8 cores were selected as research objects in this study. To account for variations in oil content, 4 samples with oil and 4 samples without oil were chosen for comparison. This study categorizes samples based on the oil-bearing classification standards for clastic rocks. Samples with visible oil traces or higher oil content are designated as oil-bearing, while those with no visible oil are designated as oil-free. The porosity and permeability tests, X-ray diffraction (XRD) analysis of the whole rock and clay minerals, and high-pressure mercury injection tests were conducted at the Experimental Center of the Research Institute of Exploration and Development of PetroChina.

To determine the fractal dimension of the pore throat structure in each porous solid sample, a capillary model based on a high-pressure mercury injection experiment was employed in our previous paper (Li et al., 2017). By analysing the relationship between the pore diameter and capillary pressure, as well as between the pore diameter and mercury saturation, the following model was derived:

$$\lg(1 - S_{\mathrm{Hg}}) = (D - 3)\lg P_{\min} - (D - 3)\lg P_{\mathrm{c}}$$

where $P_{\min}$ represents the capillary pressure corresponding to the maximum pore diameter in the reservoir (i.e., entry capillary pressure) and S_{Hg} denotes the mercury saturation at capillary pressure P_{c}. Thus, the fractal geometric formula describing the reservoir capillary pressure curve was obtained.

According to fractal theory, the fractal characteristics of pore throat structures are generally classified as overall fractal (single fractal) or segmented fractal (multifractal) characteristics (Sadeghi, 2024). The overall fractal characteristic refers to a curve on the log-log coordinate diagram of lg P_{c} and lg(1−S_{Hg}) that is a complete or nearly straight line, indicating minimal differences in the pore throat structure between large and small pores with identical fractal dimensions (Li et al., 2017). A segmented fractal characteristic, on the other hand, refers to a nonlinear curve on the log-log coordinate diagram of lg P_{c} and lg(1−S_{Hg}), featuring distinct

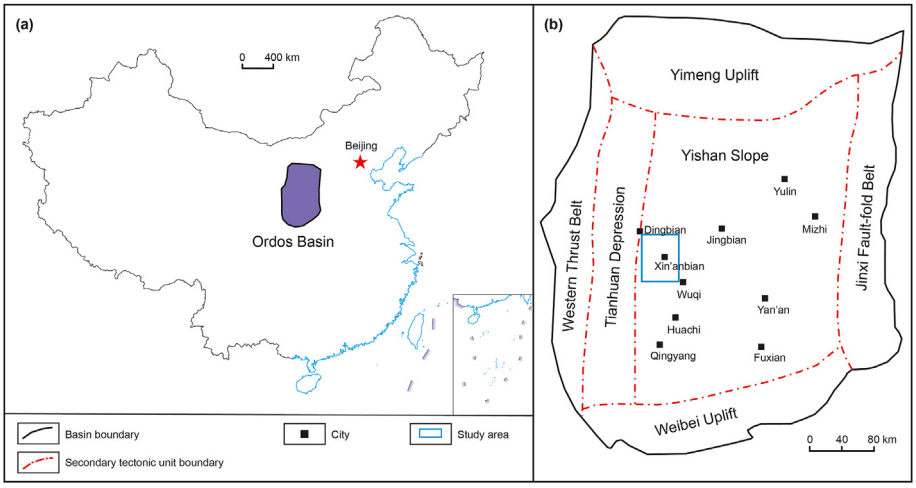

Fig. 1. Regional overview of the Ordos Basin, China (modified after Li et al., 2017)).

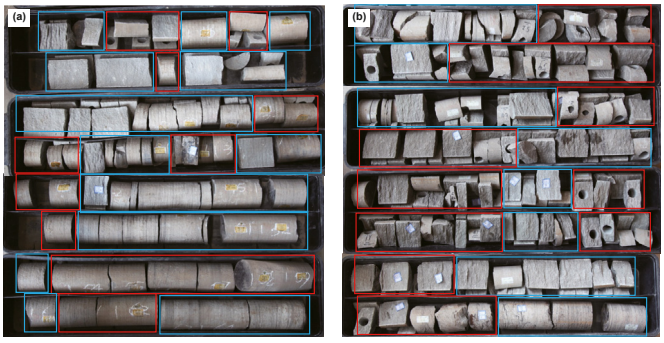

Fig. 2. Interbedded oil-bearing (red lines) and oil-free (blue lines) sandstones in the Chang 7 Member.
(**a**) Well A, 2138–2144.04 m core; (**b**) Well B, 2193.92–2208.22 m core.

Table 1
Characteristics of the porosity and permeability of the oil-bearing and oil-free samples.

Sample number	Oil content	Porosity, %	Permeability, $\times 10^{-3}$ μm^2
1	Oil-bearing	5.95	0.046
2	Oil-bearing	6.75	0.056
3	Oil-bearing	10.23	0.133
4	Oil-bearing	9.35	0.090
Average		8.07	0.0813
5	Oil-free	5.88	0.021
6	Oil-free	3.68	0.009
7	Oil-free	4.08	0.009
8	Oil-free	4.20	0.016
Average		4.46	0.0138

turning points that correspond to changes in the aperture range. This implies varying fractal dimensions for large and fine pore throats, necessitating the use of segmented regression analysis for accurate determination of these dimensions (Chang et al., 2022). This approach ensures data integrity while capturing both the distribution pattern and multifractal nature of pore throat structures. For this type of segmented fractal pore throat, calculating the weighted average mercury saturation across different scales can yield a weighted fractal dimension representing the pore throat structure of the reservoir rock.

4. Results

4.1. Porosity and permeability

The porosity and permeability characteristics of the tight sandstone of Chang 7 Member exhibit a strong positive correlation, indicating their interdependent nature in controlling fluid flow within the reservoir. However, a detailed analysis reveals distinct zonation patterns in the porosity distributions of oil-bearing and oil-free samples, reflecting variations in fluid storage and transport properties. In oil-bearing samples, porosity values range from 5.95% to 10.23%, with an average of 8.07%. Correspondingly, permeabilities span from 0.046 $\times$ 10^{-3} to 0.133 $\times$ 10^{-3} μm^2, averaging at 0.081 $\times$ 10^{-3} μm^2 (Table 1). These figures indicate a relatively higher capacity for fluid storage and movement within the porous network of oil-bearing formations. Conversely, oil-free samples display porosity levels between 3.68% and 5.88%, averaging at 4.46%. Permeability in these rocks ranges from 0.009 $\times$ 10^{-3} to 0.021 $\times$ 10^{-3} μm^2, with an average value of approximately 0.014 $\times$ 10^{-3} μm^2 (Table 1). This lower porosity and permeability in oil-free samples suggest a reduced ability to store and transmit fluids compared to their oil-bearing counterparts. The data highlights a significant difference in the reservoir quality between oil-bearing and oil-free zones, with the former exhibiting superior porosity and permeability characteristics conducive to efficient hydrocarbon production and recovery.

4.2. Mineral composition characteristics

XRD analysis reveals significant differences in mineral composition between oil-bearing and oil-free samples from the tight reservoir of Chang 7 Member. Both sample types primarily consist of quartz, plagioclase, and clay minerals, but their proportions vary markedly (Table 2). In oil-bearing samples, quartz content ranges from 21.9% to 34.1% (average 28.2%), significantly higher than the 13.1%–28.4% (average 19.4%) in oil-free samples. Potassium feldspar content in oil-bearing samples ranges from 4.7% to 10.1% (average 6.9%), compared to 3.9%–8.1% (average 6.4%) in oil-free samples. Similarly, plagioclase content in oil-bearing samples is higher, ranging from 23.8% to 30.5% (average 27.5%), than in oil-free samples, which range from 20.9% to 22.6% (average 21.5%). Calcite content is significantly lower in oil-bearing samples (0.0%–18.3%,

Table 2
Characteristics of the mineral compositions of the oil-bearing and oil-free samples.

Sample number	Quartz	Feldspar	Plagioclase	Calcite	I/S	I	K	C
1	34.1	6.0	23.8	4.1	13.8	1.0	5.4	11.8
2	27.6	6.6	30.5	18.3	4.6	0.7	6.8	4.9
3	21.9	10.1	27.1	0.0	11.9	1.2	8.6	19.2
4	30.5	4.7	28.4	0.6	5.0	2.5	1.8	26.5
Average	28.5	6.9	27.5	5.8	8.8	1.3	5.7	15.6
5	28.4	6.6	20.9	5.7	17.3	1.5	7.7	11.9
6	13.1	8.1	20.9	51.8	1.3	0.4	2.9	1.5
7	17.7	3.9	21.7	34.8	7.9	0.9	2.2	11.0
8	18.5	6.9	22.6	34.6	7.3	2.6	1.4	6.1
Average	19.4	6.4	21.5	31.7	8.4	1.4	3.5	7.6

average 5.8%) compared to oil-free samples (5.7%–51.8%, average 31.7%). Clay minerals also exhibit distinct patterns. In oil-bearing samples, total clay mineral content ranges from 17.0% to 40.9% (average 31.4%), while in oil-free samples, it ranges from 6.1% to 38.4% (average 20.95%). Chlorite is predominant in oil-bearing samples, ranging from 4.9% to 26.5% (average 15.6%), compared to 1.5%–11.9% (average 7.6%) in oil-free samples. Illite-smectite mixed-layer clay is also higher in oil-bearing samples (4.6%–13.8%, average 8.8%) compared to oil-free samples (1.3%–17.3%, average 8.4%). Overall, the presence of oil is associated with increased quartz, plagioclase, and chlorite contents, and decreased calcite levels, highlighting the significant impact of oil on the reservoir's composition.

4.3. Characteristics of the pore throat structure

Based on the morphology of the capillary pressure curves, the oil-bearing samples exhibited relatively low mercury entry pressures and median pressures, but generally high maximum mercury saturation and residual mercury saturation (Fig. 3).

By comparing the pore throat distribution characteristics of the oil-bearing and oil-free samples (Fig. 4), it was observed that samples exhibited unimodal and bimodal pore throat radius distribution curves, with significantly different peaks between the two groups. The boundary was determined to be 0.07 μm: main peaks for the oil-bearing samples were all greater than 0.07 μm, while peaks for the oil-free samples were generally less than 0.07 μm.

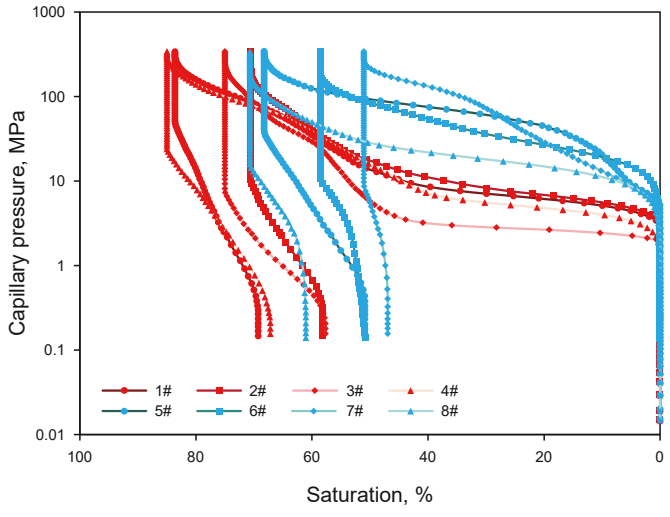

Fig. 3. High-pressure mercury injection capillary force curves for oil-bearing and oil-free samples (Red represent oil-bearing samples, while blue denote oil-free samples).

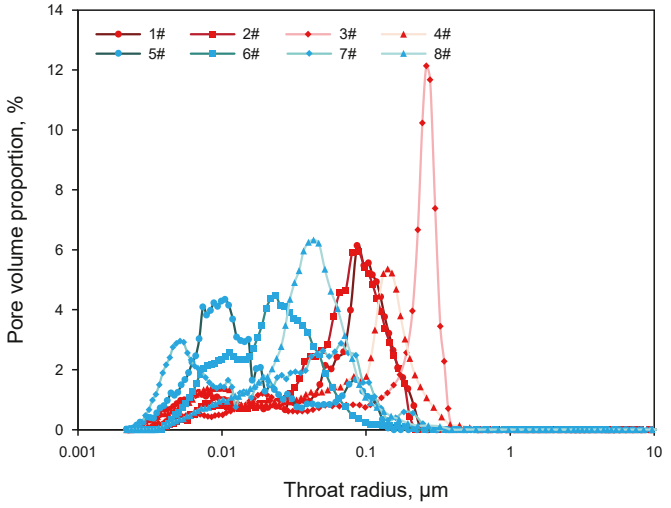

Fig. 4. Pore throat radius distribution curves of the oil-bearing and oil-free samples (Red represent oil-bearing samples, while blue denote oil-free samples).

Furthermore, there was a noticeable difference in the entire throat radius range below 0.5 μm between the two groups. Pore throat distribution analysis revealed two distinct characteristics for the oil-bearing samples: a relatively low distribution of pore throats smaller than 0.05 μm and a concentrated distribution range for pore throats larger than 0.05 μm, displaying symmetric behavior around their peak values. In contrast, the oil-free samples exhibited very low radius of pore throats less than 0.1 μm, with wide-ranging distributions characterized by complex patterns.

The analysis of mercury injection curves and pore throat distribution in the tight reservoir of Chang 7 Member unveils significant disparities between oil-bearing and oil-free samples (Table 3). Oil-bearing samples exhibit distinctive characteristics, including lower entry pressures (1.19–3.32 MPa, average 2.27 MPa), larger maximum pore throat radii (0.222–0.616 μm, average 0.376 μm), lower median pressures (5.75–17.42 MPa, average 13.19 MPa), and larger median pore throat radii (0.042–0.28 μm, average 0.067 μm) compared to oil-free samples. This suggests that oil-bearing formations possess wider pore throats and require less pressure for fluid entry and flow. Moreover, the main pore throat radius in oil-bearing samples (0.126–0.278 μm, average 0.173 μm) is notably larger than in oil-free samples (0.047–0.212 μm, average 0.108 μm). This larger pore throat radius in oil-bearing formations indicates a higher potential for fluid flow and storage within the reservoir rocks. The skewness values further differentiate the two sample types, with oil-bearing samples exhibiting higher skewness (0.48–0.83, average 0.61) compared to oil-free samples (−0.37 to

Table 3
High-pressure mercury intrusion characteristic parameters of the tight sandstones of Chang 7 Member.

Sample number	Entry pressure, MPa	Maximum throat radius, μm	Median pressure, MPa	Median radius, μm	Main throat radius, μm	Skewness	Maximum mercury saturation, %	Mercury removal efficiency, %	Effective porosity, %
1	2.74	0.269	13.70	0.054	0.126	0.60	83.62	17.17	4.97
2	3.32	0.222	17.42	0.042	0.126	0.48	70.58	17.56	4.76
3	1.85	0.398	5.75	0.128	0.278	0.83	75.01	23.14	7.67
4	1.19	0.616	15.89	0.046	0.162	0.52	85.00	20.98	7.95
Average	2.27	0.376	13.19	0.067	0.173	0.61	78.55	19.71	6.34
5	4.70	0.156	92.38	0.008	0.110	−0.37	68.22	25.46	4.01
6	5.62	0.131	84.32	0.009	0.047	0.10	58.57	13.29	2.16
7	2.48	0.296	216.15	0.003	0.212	−0.14	51.07	8.11	2.08
8	1.87	0.394	28.23	0.026	0.063	0.24	70.67	13.60	2.96
Average	3.67	0.244	105.27	0.012	0.108	−0.04	62.13	15.12	2.80

0.24, average −0.04). This higher skewness in oil-bearing formations signifies a more favorable distribution of pore throat sizes, enhancing the reservoir's fluid storage and percolation capacity. Additionally, oil-bearing samples demonstrate higher maximum mercury saturation (70.58%–85.00%, average 78.55%), higher effective porosity (4.76%–7.95%, average 6.34%), and greater mercury removal efficiency (17.17%–23.14%, average 19.71%) compared to oil-free samples. These findings collectively indicate that oil-bearing formations have superior fluid flow properties and storage potential within the tight reservoir of Chang 7 Member, making them more conducive to efficient hydrocarbon recovery and production.

4.4. Fractal characteristics

The Hodot pore classification standard delineated pore throats into distinct categories: micropores (<10 nm), transition pores (10–100 nm), mesopores (100–1000 nm), and large pores (>1000 nm) (Hodot, 1966). To evaluate fractal characteristics across scales, the lg P_c - lg(1 − S_{Hg}) diagram (Fig. 5) segregated samples into three segments based on curve morphology and the lower mercury injection threshold for pore throats: micropores (<10 nm) with a fractal dimension D3, transition pores (10–100 nm) with a fractal dimension D2, and mesopores (100–1000 nm) with a fractal dimension D1. In the oil-bearing samples, the fractal dimension D1 ranged from 2.37 to 2.66 (average 2.56), D2 ranged from 2.70 to 2.80 (average 2.74), and D3 ranged from 2.46 to 2.87 (average 2.66). The overall pore throat structure's total dimension (D) was obtained through weighted averaging and ranged from 2.51 to 2.69 (average 2.62). For oil-free samples, D1 varied from 2.93 to 2.99 (average 2.97), D2 ranged from 2.49 to 2.86 (average 2.72), and D3 ranged from 2.57 to 2.81 (average 2.69). The total dimension (D) spanned from 2.54 to 2.79 (average 2.69). Notably, the key divergence in fractal attributes between oil-bearing and oil-free samples primarily stemmed from D1. The oil-free samples displayed D1 values approaching 3, indicating highly non-uniform pore throat structures at this scale. Conversely, differences in D2 and D3 were relatively minor, underscoring the pivotal role of D1 in dictating overall fractal characteristics.

We conducted a detailed statistical analysis of porosity distribution across different pore throat scales in various samples and calculated their corresponding contributions to permeability (Table 4). In oil-bearing samples, the average porosity was 3.07%, with an average permeability contribution of 0.07335 × 10^{-3} μm^2. Transition pores exhibited an average porosity of 2.41%, contributing 0.00786 × 10^{-3} μm^2 to permeability. Micropores had an average porosity of 0.86%, with a minimal permeability contribution of 0.00003 × 10^{-3} μm^2. In contrast, oil-free samples showed an average porosity of 0.09% and an associated permeability

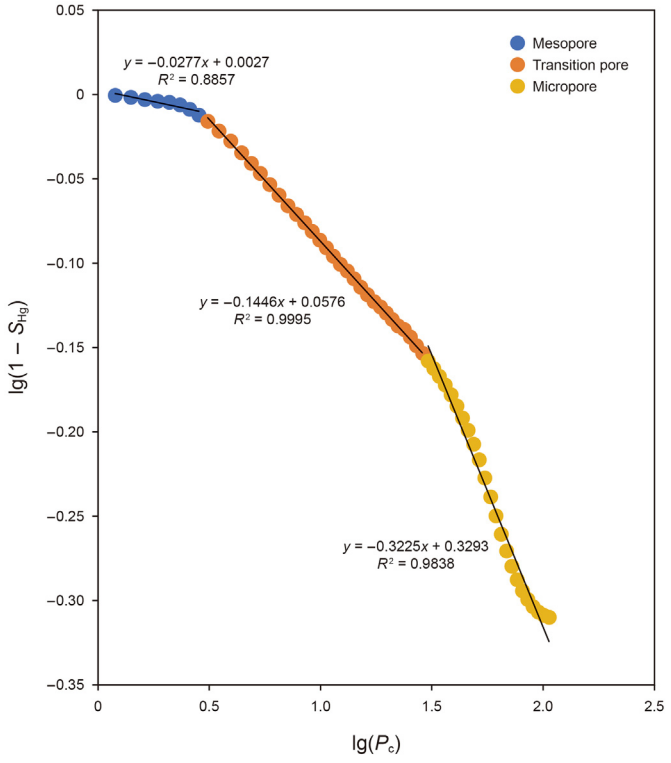

Fig. 5. Fractal dimension characteristic curve of sample #7.

contribution of 0.00503 × 10^{-3} μm^2. Transition pores in oil-free samples had an average porosity of 1.85%, contributing 0.00855 × 10^{-3} μm^2 to permeability. Micropores in oil-free samples, with an average porosity identical to oil-bearing samples (0.86%), exhibited a slightly higher permeability contribution of 0.00017 × 10^{-3} μm^2. The most significant disparity between oil-bearing and oil-free samples was observed at the mesopore scale. Here, the porosity and permeability of oil-free samples were more than an order of magnitude smaller than those of oil-bearing samples. This highlights the critical role of mesopores in determining the superior permeability and storage capacity of oil-bearing formations.

5. Discussion

5.1. The relationship between oil content and micro pore throat structure

Micro- and nanopore throat systems are extensively developed

Table 4
Calculation results for the fractal dimension and statistical table of the contribution values of the pore throat porosity and permeability at different scales.

Sample number	D	D1	D2	D3	Volume corresponding to D1	Volume corresponding to D2	Volume corresponding to D3	Contribution value of permeability of D1	Contribution value of permeability of D2	Contribution value of permeability of D3
1	2.63	2.58	2.73	2.48	1.78	2.25	0.94	0.03653	0.00943	0.00004
2	2.69	2.63	2.70	2.87	1.48	2.88	0.40	0.03954	0.01643	0.00003
3	2.51	2.37	2.80	2.82	5.25	1.82	0.60	0.13174	0.00125	0.00001
4	2.65	2.66	2.73	2.46	3.77	2.68	1.49	0.08561	0.00434	0.00005
Average	2.62	2.56	2.74	2.66	3.07	2.41	0.86	0.07335	0.00786	0.00003
5	2.72	2.93	2.84	2.57	0.13	2.03	1.85	0.00826	0.01226	0.00048
6	2.71	2.99	2.70	2.71	0.02	1.66	0.48	0.00182	0.00705	0.00013
7	2.79	2.97	2.86	2.68	0.11	1.10	0.87	0.00460	0.00435	0.00006
8	2.54	2.98	2.49	2.81	0.11	2.60	0.26	0.00544	0.01053	0.00003
Average	2.69	2.97	2.72	2.69	0.09	1.85	0.86	0.00503	0.00855	0.00017

in tight reservoirs, characterized by small pore throats. In these reservoirs, the buoyancy of oil droplets is significantly lower than the substantial capillary resistance generated by the capillary pore throats. Consequently, natural gravity differentiation between oil and water becomes challenging due to the limited buoyancy. As a result, buoyancy ceases to be the primary driving force for oil migration in tight reservoirs, leading to complex heterogeneity in oil-bearing properties (Zheng et al., 2016).

High-pressure mercury injection analysis of various oil-bearing samples revealed that the pore throat distribution and permeability contribution curves of samples with high oil content exhibited remarkable consistency (Fig. 6). The pore volume distribution showed a slight bimodal pattern, with the primary peak between 100 and 300 nm and a secondary peak around 10 nm. The permeability contribution displayed a distinct unimodal pattern, closely aligning with the primary peak of the pore volume distribution curve. The overlap plot of the cumulative pore volume distribution and cumulative permeability contribution curves further demonstrated a two-stage characteristic: an initial slow increase followed by a rapid rise for the pore volume distribution, whereas the permeability contribution curve increased rapidly within a smaller pore size range, starting at the inflection point of the two-stage pore volume distribution curve (Fig. 7).

In contrast, oil-free samples displayed notable discrepancies in peak alignment within their pore throat distribution and permeability contribution curves. The pore volume distribution exhibited both unimodal and bimodal patterns (Fig. 8). The unimodal peaks were all smaller than 100 nm, while the bimodal peaks were smaller than 10 nm and 100 nm, respectively. The permeability contribution also showed both unimodal and bimodal patterns, but their peaks generally did not align with the primary peaks of the pore volume distribution curves. Their cumulative curves exhibited distinct characteristics: the pore volume cumulative distribution curve initially increased rapidly and then slowly, while the permeability contribution cumulative curve increased over a wider pore size distribution range (Fig. 9).

These observations underscore the significant influence of pore throat connectivity on oil presence within tight reservoirs. Unlike conventional reservoirs, tight sandstone reservoirs are characterized by small pore throats and the development of numerous nanoscale pore throats, resulting in pronounced complexity and heterogeneity in pore structure. This complexity leads to significant

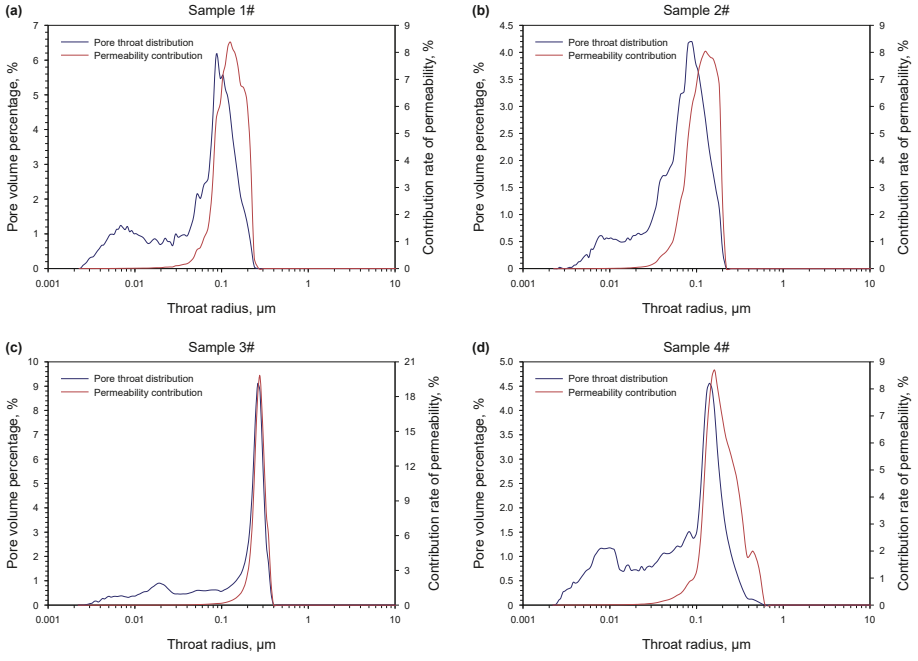

Fig. 6. Overlap plot of the pore throat radius distribution curves and permeability contribution curves for the oil-bearing samples.

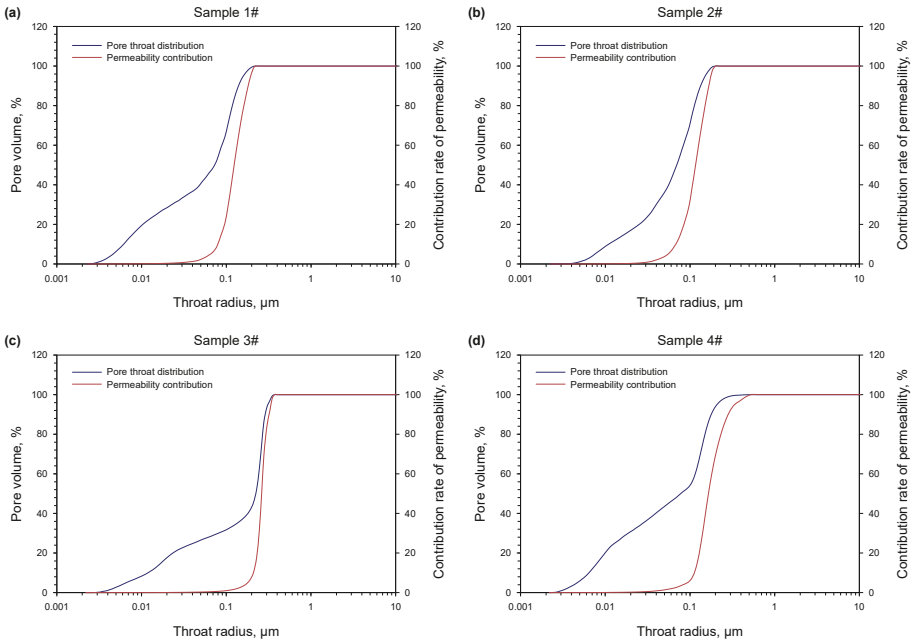

Fig. 7. Overlap plot of cumulative distribution curve of pore volume and cumulative contribution curve of permeability for the oil-bearing samples.

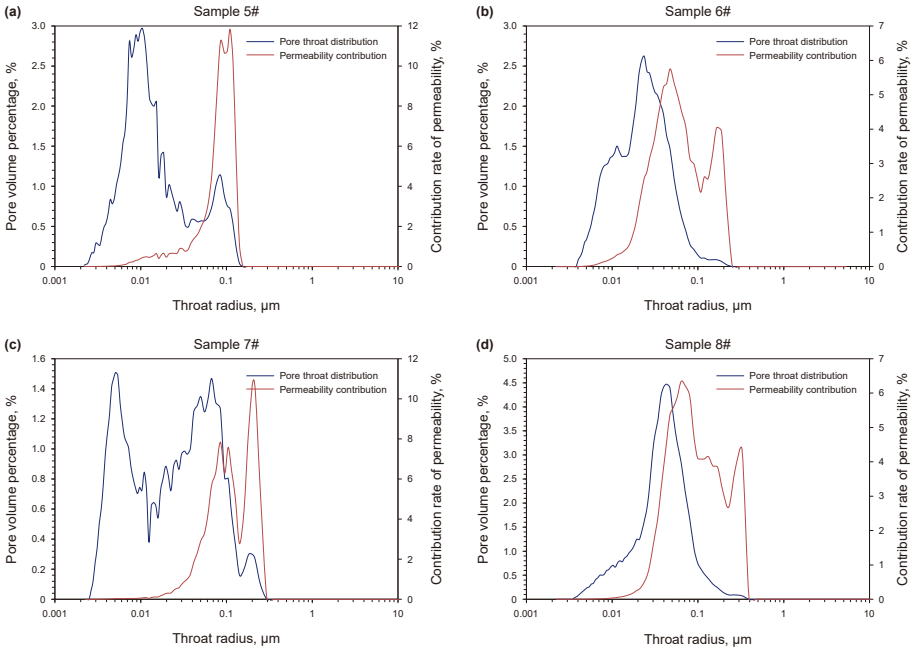

Fig. 8. Overlap plot of the pore throat radius distribution curves and permeability contribution curves for the oil-free samples.

variations in oil enrichment within tight reservoirs. The microscopic pore structure controls the storage and flow capacity of hydrocarbons, thereby determining the effectiveness of oil accumulation and migration within the micro-nano pore throat system.

Additionally, this analysis revealed a clear zoning pattern in parameters like median radius and skewness between these two sample types. Oil-bearing samples showed larger median radii, generally exceeding 0.04 μm, along with higher skewness values indicative of partial skewness, highlighting their robust seepage capacity. Conversely, oil-free samples displayed smaller median radii and lower skewness values, reflecting comparatively weaker overall seepage capacities (Fig. 10). This observation suggests that not all pore systems can accommodate oil; rather, only those compatible with the charging power can effectively hold it. As a result, tight sandstone reservoirs exhibit heterogeneity in oil occurrence due to this selective filling process. Nelson's investigation of clastic reservoirs with varying grain sizes enabled the determination of throat diameter distributions for conventional and tight sandstone reservoirs, as well as the diameter range for various organic molecules from asphaltene to methane (Nelson, 2009). Furthermore, theoretical calculations and simulation experiments on oil displacement and water charging processes by

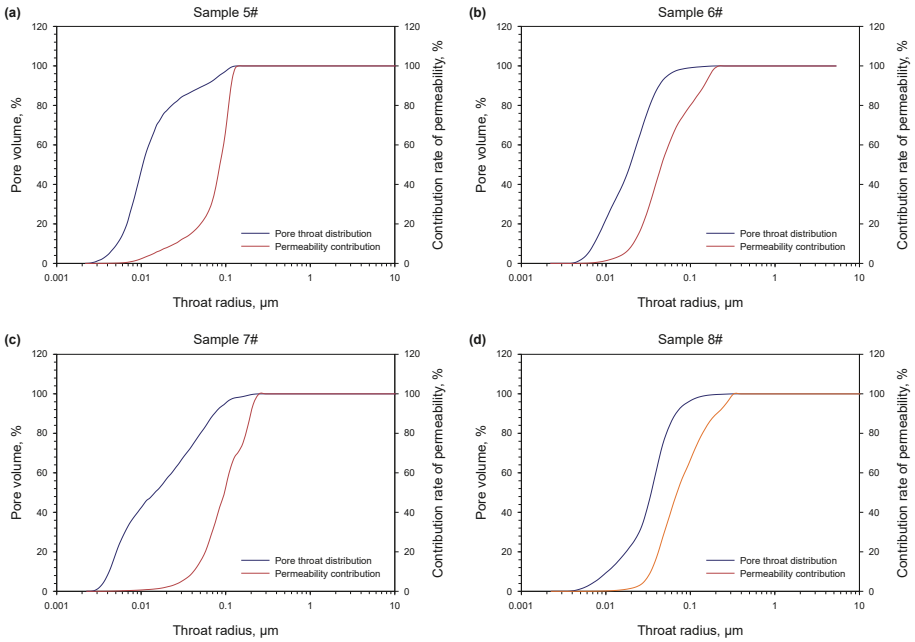

Fig. 9. Overlap plot of cumulative distribution curve of pore volume and cumulative contribution curve of permeability for the oil-free samples.

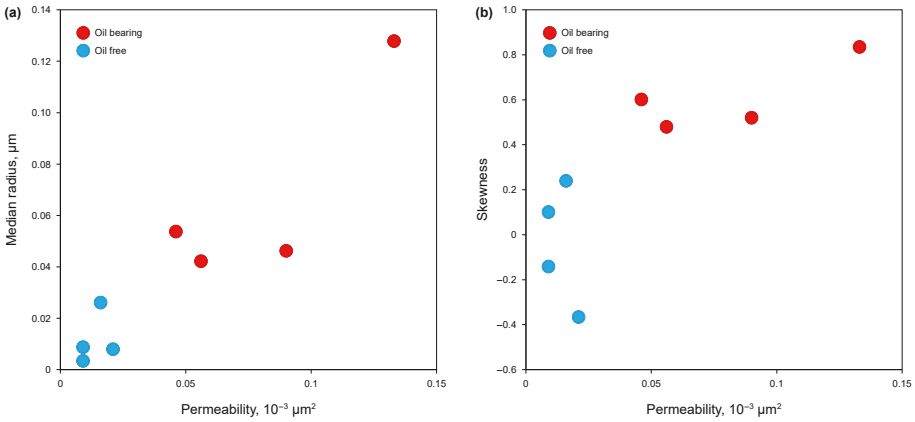

Fig. 10. Relationships between the median radius, skewness, and permeability of oil-bearing and oil-free samples.

other researchers have corroborated that the lower limit of oil occurrence in tight reservoirs typically falls within the range of 20–60 nm—a finding consistent with our findings in this study area (Zou et al., 2012; Li et al., 2022a).

5.2. Relationship between physical properties and fractal dimension under different oil conditions

The physical properties of reservoirs are influenced not only by the inherent characteristics of the rock but also by the intricate structure of pore throats. A significant negative correlation emerged between the fractal dimension of pore throats with different dimensions and their corresponding porosity (R^2 values are 0.812, 0.3596, and 0.597) (Fig. 11). As the occupied pore space decreased, the fractal dimension of each scale increased, while the porosities of pore throats with different dimensions tended to converge at a certain point with increasing fractal dimension. This indicates that pore throats of varying sizes strongly control their respective fractal dimensions in reservoirs. The relationship between the fractal dimension of pore throats and their corresponding permeability is intricate. Only mesopore throats exhibit a strong negative correlation with permeability ($R^2 = 0.8647$), while the fractal dimensions of transition pores and micropores show no clear correlation with permeability (Fig. 11). Hence, mesopore throats exert a significant influence on permeability. As the fractal dimension increases, the complexity of pore throat structures intensifies, leading to increased proportions of pores within reservoir spaces, greater heterogeneity, enhanced roughness on pore surfaces, deteriorated connectivity, and decreased reservoir capacity, percolation capacity, porosity, and permeability.

The total fractal dimension of the reservoir in our study area shows a negative correlation with both porosity and permeability, albeit to varying extents (Fig. 12). The stronger correlation observed with permeability ($R^2 = 0.3721$) can be attributed to the fact that the total fractal dimension is primarily influenced by pore throats that contribute significantly to porosity. However, pore throats of different scales exhibit distinct fractal dimensions, which weakens the relationship between the overall fractal dimension and total porosity. In contrast, permeability is mainly influenced by

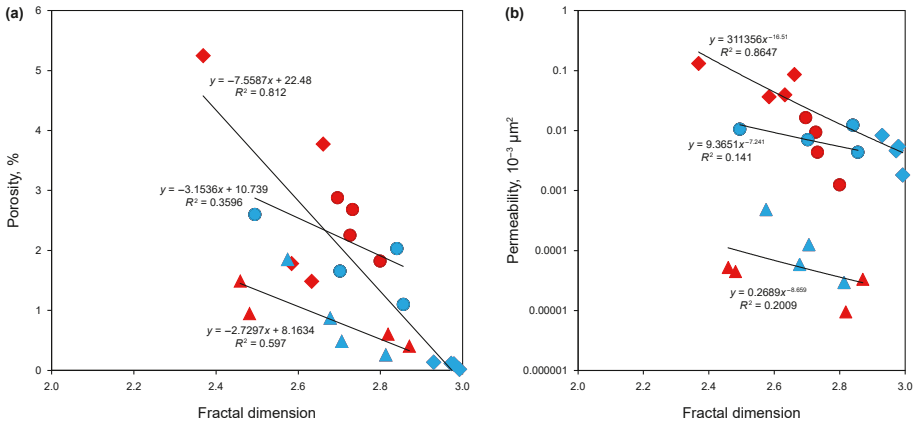

Fig. 11. Relationships between the fractal dimensions of pore throats at different scales and their corresponding porosities and permeabilities (Red represent oil-bearing samples, while blue denote oil-free samples. Diamonds correspond to mesopore throats, circles represent transition pore throats, and triangles indicate micropore throats).

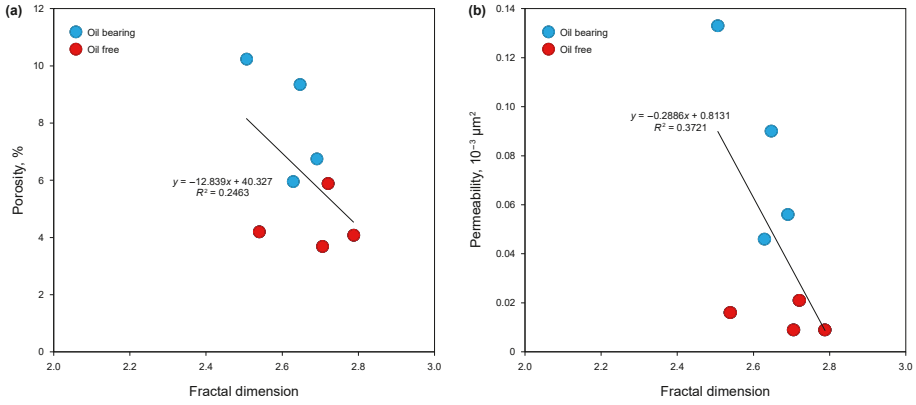

Fig. 12. Relationships between total fractal dimension and porosity and permeability.

mesopores, whereas the total fractal dimension encompasses pore throats of varying scales. As a result, the association between the fractal dimension and permeability is also affected by the collective impact of mesopores, transition pores, and micropores. This collective impact diminishes the influence of mesopores on permeability and subsequently reduces their correlation with the total fractal dimension.

In summary, the correlations between the fractal dimension of pore throsts in different sacles, total fractal dimension of the whole pore throats system, and the corresponding porosity and permeability parameters were found to be inconsistent. This underscores the complexity of the reservoir's pore throat structure regarding its fractal characteristics. Additionally, the pattern of variation in pore throat fractal dimension may vary with changes in pore throat size. However, it is clear that meso-sized pore throats have the most significant impact on seepage capacity.

5.3. Analysis of factors controlling the differences in oil content

To delve deeper into the influence of pore throat structure on fractal dimension, we delved into the correlation between the fractal dimension D1 and both the median radius and skewness (Fig. 13). The median radius signifies the pore throat radius at 50% mercury saturation, while skewness reflects the asymmetry of the pore throat size distribution. Our findings revealed a robust negative correlation ($R^2 = 0.8452$) between D1 and the median radius. This suggests that as the median radius decreases, D1 tends to increase, resulting in compromised reservoir performance. Furthermore, we observed a significant negative correlation ($R^2 = 0.7473$) between D1 and skewness. This implies that as skewness decreases, indicating a more symmetrical pore throat size distribution, D1 tends to increase. This change in skewness leads to an enhancement in D1, reflecting a more complex and less efficient pore throat structure.

To investigate the intricate dynamics shaping these phenomena, our analysis focused on elucidating the nuanced relationship between mesopore classification dimensions and mineral composition within the reservoir. These mineral variations play a pivotal role in shaping the complexity and heterogeneity of pore structures, which are manifested through shifts in fractal dimensions (Dou et al., 2018; Lai et al., 2018; Zang et al., 2022). We conducted a meticulous examination of how fractal dimensions interact with quartz, feldspar, calcite, and clay minerals, shedding light on their profound impact on reservoir heterogeneity.

The D1 parameter exhibited a negative correlation with quartz and plagioclase contents, with R^2 values of 0.2863 and 0.5479, respectively (Fig. 14). Quartz particles exhibit relative stability, resisting compaction-induced damage within pore throat systems. While localized secondary quartz enlargement may occur, mainly in the form of ring edge expansions, its impact on structural heterogeneity within the pore network remains minimal. Plagioclase, prevalent in the tight sandstone of Chang 7 Member, is prone to dissolution in an acidic environment, particularly along fractures. This dissolution process leads to the creation of secondary pores

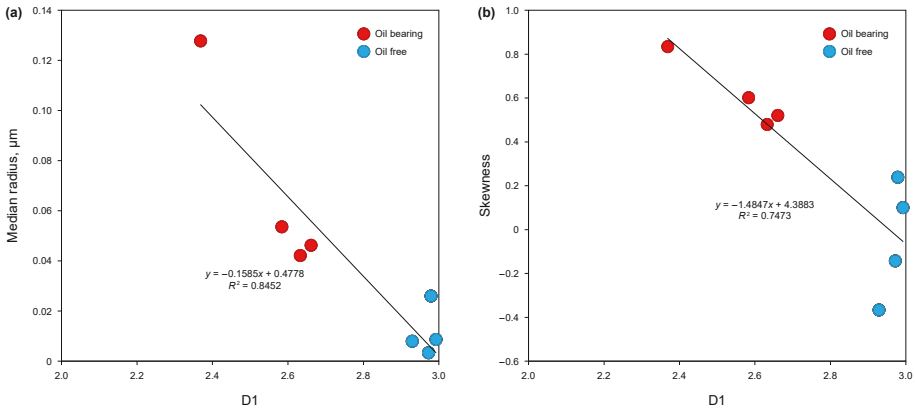

Fig. 13. Relationships between D1 and the median radius and skewness.

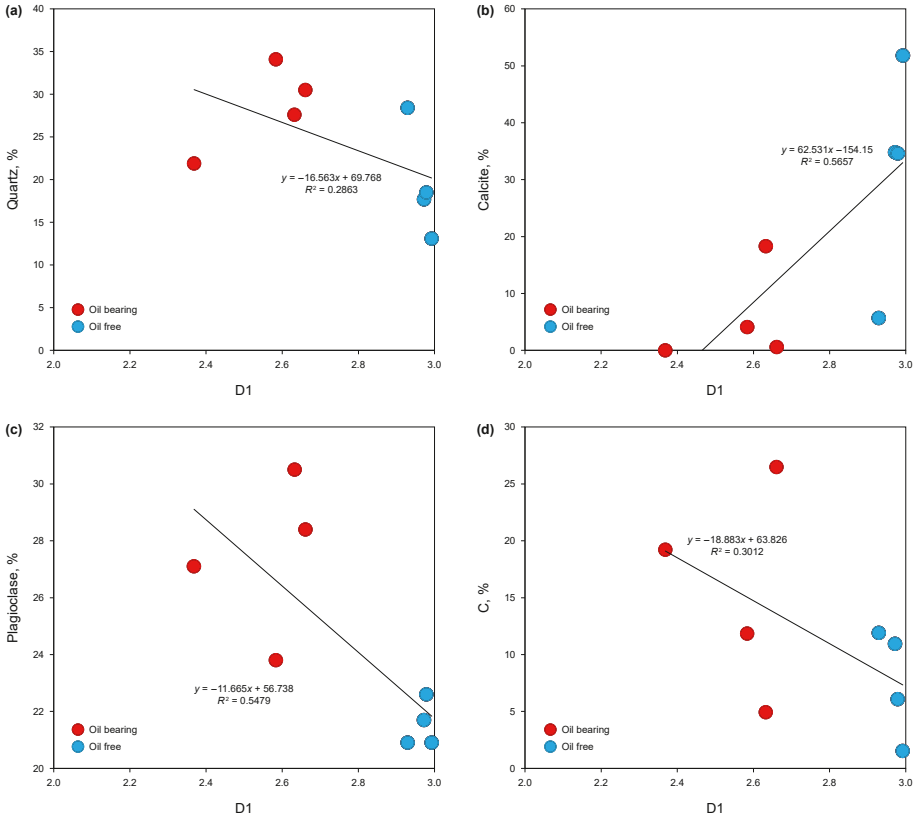

Fig. 14. Relationships between D1 and the quartz, plagioclase, and calcite chlorite contents.

that are conducive to oil and gas storage, thereby enhancing pore connectivity. Consequently, higher quartz and plagioclase contents contribute to smoother pore surfaces, simpler structures, smaller fractal dimensions, and reduced heterogeneity within the reservoir.

Moving on, D1 exhibited a positive correlation with calcite, as evidenced by an R^2 value of 0.5657. The tight sandstone of Chang 7 Member commonly displays carbonate cementation, which obstructs pore throats, alters pore shapes, reduces connectivity, compromises structure integrity, and ultimately elevates fractal dimensions.

Furthermore, D1 showcased a negative correlation with chlorite content, resulting in an R^2 of 0.3012. The tight sandstone of Chang 7 Member predominantly features needle-shaped chlorite lining the pores, hindering quartz autogenesis and resisting compaction. This characteristic fosters a more uniform distribution of pore sizes and lower fractal dimensions, indicative of reduced complexity in pore structure. In essence, this comprehensive analysis underscores the intricate interplay between mineral composition and pore structure characteristics, highlighting how variations in mineral content can significantly influence the heterogeneity and seepage capacity of tight sandstone reservoirs.

6. Conclusion

The porosity and permeability of oil-bearing samples are markedly higher than those of oil-free samples. Oil-bearing samples exhibit significantly higher concentrations of quartz, plagioclase, and chlorite, with a corresponding reduction in calcite

content. These samples also demonstrate lower mercury entry and median pressures, along with higher maximum and residual mercury saturations compared to their oil-free counterparts.

The pore throat radius distribution curves of the oil-bearing samples display both unimodal and bimodal patterns, with the main peak values exceeding 0.07 μm. In contrast, the peak values for oil-free samples generally fall below this threshold. The alignment between pore throat distribution and permeability contribution curves in oil-bearing samples highlights the importance of pore throat connectivity, a feature absent in the oil-free samples.

Minimal differences are observed in the D2 and D3 fractal dimensions between oil-bearing and oil-free samples. However, the primary distinction lies in the D1 dimension, where oil-bearing samples exhibit an average D1 of 2.56 compared to 2.97 in oil-free samples, indicating a more heterogeneous pore throat structure in the latter.

The pore throat structural nonuniformity in oil-free samples is closely tied to the volume proportion of the pore throats. The porosity and permeability of oil-free samples are more than an order of magnitude lower than those of oil-bearing samples, with mesopores playing a critical role in enhancing seepage capacity.

Quartz, plagioclase, and chlorite content show a positive correlation with D1, suggesting that their presence improves pore throat structure. Conversely, calcite content is negatively correlated with D1. The complexity of pore throat structures is further heightened by cementation, with diagenetic processes exerting control over these characteristics and influencing oil content variations.

Declaration of competing interest

The manuscript "The fractal characteristics of the pore throat structure of tight sandstone and its influence on oil content: A case study of the Chang 7 Member of the Ordos Basin, China" has not been previously published and not been currently submitted for review to other journals. The authors declare that they have no competing interests.

CRediT authorship contribution statement

Peng Li: Writing – review & editing, Writing – original draft, Visualization, Validation, Supervision, Resources, Project administration, Methodology, Investigation, Funding acquisition, Formal analysis, Data curation, Conceptualization. **Bao-Jian Shen:** Writing – review & editing, Validation, Supervision, Investigation. **Ya-Li Liu:** Writing – review & editing, Validation, Supervision, Investigation. **He Bi:** Writing – original draft, Visualization, Resources, Methodology, Data curation, Conceptualization. **Zhong-Bao Liu:** Writing – review & editing, Writing – original draft, Validation, Methodology, Investigation, Funding acquisition, Formal analysis. **Rui-Kang Bian:** Formal analysis, Data curation. **Peng-Wei Wang:** Formal analysis, Data curation. **Pei Li:** Investigation, Formal analysis.

Acknowledgments

This study was supported by the National Natural Science Foundation of China (Grant No. 42002139) and the Basic Prospective Project of SINOPEC (Grant No. P23240-3).

References

Anovitz, L.M., Cole, D.R., Rother, G., et al., 2013. Diagenetic changes in macro- to nano-scale porosity in the St. Peter Sandstone: an (ultra) small angle neutron scattering and backscattered electron imaging analysis. Geochim. Cosmochim. Ac. 102, 280–305. https://doi.org/10.1016/j.gca.2012.07.035.

Cao, Z., Jiang, H., Zeng, J., et al., 2021. Nanoscale liquid hydrocarbon adsorption on clay minerals: a molecular dynamics simulation of shale oils. Chem. Eng. J. 420, 127578. https://doi.org/10.1016/j.cej.2020.127578.

Chang, J., Fan, X., Jiang, Z., et al., 2022. Differential impact of clay minerals and organic matter on pore structure and its fractal characteristics of marine and continental shales in China. Appl. Clay Sci. 216, 106334. https://doi.org/10.1016/j.clay.2021.106334.

Dou, W., Liu, L., Wu, K., et al., 2018. Diagenetic heterogeneity, pore throats characteristic and their effects on reservoir quality of the Upper Triassic tight sandstones of Yanchang Formation in Ordos Basin. China. Mar. Petrol. Geol. 98, 243–257. https://doi.org/10.1016/j.marpetgeo.2018.08.019.

Feng, Z., Dong, D., Tian, J., et al., 2021. Geochemical characteristics of the Paleozoic natural gas in the Yichuan-Huanglong area, southeastern margin of the Ordos Basin: based on late gas generation mechanisms. Mar. Petrol. Geol. 124, 104867. https://doi.org/10.1016/j.marpetgeo.2020.104867.

Feng, Z., Hao, F., Zhou, S., et al., 2020. Pore systems of the different lithofacies of the Longmaxi formation at depths exceeding 3500 m in the zigong area, Sichuan Basin. Energ. Fuel. 34 (5), 5733–5752. https://doi.org/10.1021/acs.energyfuels.0c00456.

Ghanbarian, B., Torres-Verdín, C., Lake, L.W., et al., 2019. Gas permeability in unconventional tight sandstones: scaling up from pore to core. J. Petrol. Sci. Eng. 173, 1163–1172. https://doi.org/10.1016/j.petrol.2018.10.057.

Giri, A., Tarafdar, S., Gouze, P., et al., 2012. Fractal pore structure of sedimentary rocks: simulation in 2-d using a relaxed bidisperse ballistic deposition model. J. Appl. Geophys. 87, 40–45. https://doi.org/10.1016/j.jappgeo.2012.09.002.

Gong, Y., Liu, K., 2020. Pore throat size distribution and oiliness of tight sands-A case study of the Southern Songliao Basin, China. J. Petrol. Sci. Eng. 184, 106508. https://doi.org/10.1016/j.petrol.2019.106508.

Griffin, W.M., Stolz, J.F., Ziegler, C., 2022. Global unconventional oil and gas reserves and their development. In: Bain, D., Griffin, M., Stolz, J. (Eds.), Environmental Impacts from the Development of Unconventional Oil and Gas Reserves. Cambridge University Press, Cambridge, pp. 3–18. https://doi.org/10.1017/9781108774178.003.

Hodot, B.B., 1996. Outburst of coal and coalbed gas. In: Song, S.Z., Wang, Y.A. (Eds.), Translation, Beijing, China Ind. Pre.

Ji, W., Song, Y., Jiang, Z., et al., 2016. Fractal characteristics of nano-pores in the lower silurian longmaxi shales from the upper yangtze platform, south China. Mar. Petrol. Geol. 78, 88–98. https://doi.org/10.1016/j.marpetgeo.2016.08.023.

Jia, C.Z., Pang, X.Q., Song, Y., 2023. Whole petroleum system and ordered distribution pattern of conventional and unconventional oil and gas reservoirs. Pet. Sci. 20 (1), 1–19. https://doi.org/10.1016/j.petsci.2022.12.012.

Jia, C., 2017. Breakthrough and significance of unconventional oil and gas to classical petroleum geology theory. Petrol. Explor. Dev. 44 (1), 1–10. https://doi.org/10.1016/S1876-3804(17)30002-2.

Jia, C., Zheng, M., Zhang, Y., 2012. Unconventional hydrocarbon resources in China and the prospect of exploration and development. Petrol. Explor. Dev. 39 (2), 139–146. https://doi.org/10.1016/S1876-3804(12)60026-3.

Jiu, B., Huang, W., Li, Y., et al., 2021. Influence of clay minerals and cementation on pore throat of tight sandstone gas reservoir in the eastern Ordos Basin, China. J. Nat. Gas Sci. Eng. 87, 103762. https://doi.org/10.1016/j.jngse.2020.103762.

Lai, J., Wang, G., Wang, Z., et al., 2018. A review on pore structure characterization in tight sandstones. Earth Sci. Rev. 177, 436–457. https://doi.org/10.1016/j.earscirev.2017.12.003.

Li, C., Lin, M., Ji, L., et al., 2019a. Multiphase flow in tight sandstone: an improved application for 3D intermingled fractal model. J. Petrol. Sci. Eng. 177, 403–414. https://doi.org/10.1016/j.petrol.2019.02.030.

Li, C., Liu, G., Cao, Z., et al., 2022a. Oil charging pore throat threshold and accumulation effectiveness of tight sandstone reservoir using the physical simulation experiments combined with NMR. J. Petrol. Sci. Eng. 208, 109338. https://doi.org/10.1016/j.petrol.2021.109338.

Li, M., Qu, Z., Wang, M., et al., 2023. The influence of micro-heterogeneity on water injection development in low-permeability sandstone oil reservoirs. Minerals 13 (12), 1533. https://doi.org/10.3390/min13121533.

Li, P., Jia, C., Jin, Z.Q., et al., 2020. Pore size distribution of a tight sandstone reservoir and its effect on micro pore-throat structure: a case study of the Chang 7 member of the xin'anbian block, Ordos Basin, China. Acta Geol. Sin. - Engl. 94 (2), 219–232. https://doi.org/10.1111/1755-6724.14288.

Li, P., Jia, C., Jin, Z., et al., 2019b. The characteristics of movable fluid in the Triassic lacustrine tight oil reservoir: a case study of the Chang 7 member of Xin'anbian Block, Ordos Basin. China. Mar. Petrol. Geol. 102, 126–137. https://doi.org/10.1016/j.marpetgeo.2018.11.019.

Li, P., Liu, Z., Bi, H., et al., 2022b. Fractal characteristics of the micropore throats in the shale oil reservoirs of the Chang 7 member of the Yanchang Formation, Ordos Basin. Interpretation 10 (3), SD47–SD59. https://doi.org/10.1190/int-2021-0162.1.

Li, P., Zheng, M., Bi, H., et al., 2017. Pore throat structure and fractal characteristics of tight oil sandstone: a case study in the Ordos Basin, China. J. Petrol. Sci. Eng. 149, 665–674. https://doi.org/10.1016/j.petrol.2016.11.015.

Liu, Q., Chen, M., Liu, W., et al., 2009. Origin of natural gas from the Ordovician paleo-weathering crust and gas-filling model in Jingbian gas field, Ordos basin, China. J. Asian Earth Sci. 35 (1), 74–88. https://doi.org/10.1016/j.jseaes.2009.01.005.

Liu, Q., Jin, Z., Liu, W.L., et al., 2013. Presence of carboxylate salts in marine carbonate strata of the Ordos Basin and their impact on hydrocarbon generation

evaluation of low TOC, high maturity source rocks. Sci. China Earth Sci. 56 (12), 2141–2149. https://doi.org/10.1007/s11430-013-4713-3.
Liu, Q., Jin, Z., Meng, Q., et al., 2015. Genetic types of natural gas and filling patterns in Daniudi gas field, Ordos Basin, China. J. Asian Earth Sci. 107, 1–11. https://doi.org/10.1016/j.jseaes.2015.04.001.
Liu, Q., Li, P., Jin, Z., et al., 2022. Organic-rich formation and hydrocarbon enrichment of lacustrine shale strata: a case study of Chang 7 Member. Sci. China Earth Sci. 65 (1), 118–138. https://doi.org/10.1007/s11430-021-9819-y.
Loucks, R.G., Reed, R.M., Ruppel, S.C., et al., 2009. Morphology, genesis, and distribution of nanometer-scale pores in siliceous mudstones of the mississippian barnett shale. J. Sediment. Res. 79 (12), 848–861. https://doi.org/10.2110/jsr.2009.092.
Ma, Z., Tan, J., Zheng, L., et al., 2022. Simulation experiment of fluid-feldspar sandstone interactions and their implications for tight oil and gas exploration of the Yanchang Formation, Ordos Basin. China. Mar. Petrol. Geol. 142, 105737. https://doi.org/10.1016/j.marpetgeo.2022.105737.
Male, F., Duncan, I.J., 2022. The paradox of increasing initial oil production but faster decline rates in fracking the Bakken Shale: implications for long term productivity of tight oil plays. J. Petrol. Sci. Eng. 208, 109406. https://doi.org/10.1016/j.petrol.2021.109406.
Mandelbrot, B.B., Passoja, D.E., Paullay, A.J., 1984. Fractal character of fracture surfaces of metals. Nature 308 (5961), 721–722. https://doi.org/10.1038/308721a0.
Nelson, P.H., 2009. Pore-throat sizes in sandstones, tight sandstones, and shales. AAPG Bull. 93 (3), 329–340. https://doi.org/10.1306/10240808059.
Pfeifer, P., 1984. Fractal dimension as working tool for surface-roughness problems. Appl. Surf. Sci. 18 (1), 146–164. https://doi.org/10.1016/0378-5963(84)90042-4.
Ramiro-Ramirez, S., Bhandari, A.R., Reed, R.M., et al., 2024. Permeability of upper Wolfcamp lithofacies in the Delaware Basin: the role of stratigraphic heterogeneity in the production of unconventional reservoirs. AAPG Bull. 108 (2), 293–326. https://doi.org/10.1306/12202222033.
Sadeghi, B., 2024. Fractals and Multifractals in the Geosciences. Elsevier. https://doi.org/10.1016/C2020-0-03441-9.
Schlueter, E.M., Zimmerman, R.W., Witherspoon, P.A., et al., 1997. The fractal dimension of pores in sedimentary rocks and its influence on permeability. Eng. Geol. 48 (3), 199–215. https://doi.org/10.1016/S0013-7952(97)00043-4.
Velasco, R., Panja, P., Pathak, M., et al., 2018. Analysis of north-American tight oil production. AIChE J. 64 (4), 1479–1484. https://doi.org/10.1002/aic.16034.
Wachtmeister, H., Lund, L., Aleklett, K., et al., 2017. Production decline curves of tight oil wells in Eagle Ford shale. Nat. Resour. Res. 26 (3), 365–377. https://doi.org/10.1007/s11053-016-9323-2.
Wang, H., Ma, F., Tong, X., et al., 2016a. Assessment of global unconventional oil and gas resources. Petrol. Explor. Dev. 43 (6), 925–940. https://doi.org/10.1016/S1876-3804(16)30111-2.
Wang, P., Jiang, Z., Ji, W., et al., 2016b. Heterogeneity of intergranular, intraparticle and organic pores in Longmaxi shale in Sichuan Basin, South China: evidence from SEM digital images and fractal and multifractal geometries. Mar. Petrol. Geol. 72, 122–138. https://doi.org/10.1016/j.marpetgeo.2016.01.020.
Wang, T., Philp, R.P., 2019. Oil families and inferred source rocks of the Woodford–Mississippian tight oil play in northcentral Oklahoma. AAPG Bull. 103 (4), 871–903. https://doi.org/10.1306/09181818049.
Xi, K., Cao, Y., Liu, K., et al., 2019. Geochemical constraints on the origins of calcite cements and their impacts on reservoir heterogeneities: a case study on tight oil sandstones of the Upper Triassic Yanchang Formation, southwestern Ordos Basin, China. AAPG Bull. 103 (10), 2447–2485. https://doi.org/10.1306/01301918093.
Yang, G., Huang, D., Huang, P., et al., 2017. Control factors of high and stable production of Jurassic Da'anzhai Member tight oil in central Sichuan Basin, SW China. Petrol. Explor. Dev. 44 (5), 866–875. https://doi.org/10.1016/S1876-3804(17)30098-8.
Yang, Y.B., Xiao, W.L., Zheng, L.L., et al., 2023. Pore throat structure heterogeneity and its effect on gas-phase seepage capacity in tight sandstone reservoirs: a case study from the Triassic Yanchang Formation, Ordos Basin. Pet. Sci. 20 (5), 2892–2907. https://doi.org/10.1016/j.petsci.2023.03.020.
Zang, Q., Liu, C., Awan, R.S., et al., 2022. Occurrence characteristics of the movable fluid in heterogeneous sandstone reservoir based on fractal analysis of NMR data: a case study of the Chang 7 Member of Ansai Block, Ordos Basin, China. J. Petrol. Sci. Eng. 214, 110499. https://doi.org/10.1016/j.petrol.2022.110499.
Zheng, M., Li, J., Wu, X., et al., 2016. Physical modeling of oil charging in tight reservoirs: a case study of permian lucaogou formation in jimsar sag, junggar basin, NW China. Petrol. Explor. Dev. 43 (2), 241–250. https://doi.org/10.1016/S1876-3804(16)30027-1.
Zhu, J., Zhang, R., Zhang, Y., et al., 2019. The fractal characteristics of pore size distribution in cement-based materials and its effect on gas permeability. Sci. Rep. 9 (1), 17191. https://doi.org/10.1038/s41598-019-53828-5.
Zou, C., Guo, Q., Yang, Z., et al., 2019. Resource potential and core area prediction of lacustrine tight oil: the Triassic Yanchang Formation in Ordos Basin, China. AAPG Bull. 103 (6), 1493–1523. https://doi.org/10.1306/11211816511.
Zou, C., Yang, Z., Tao, S., et al., 2012. Nano-hydrocarbon and the accumulation in coexisting source and reservoir. Petrol. Explor. Dev. 39 (1), 15–32. https://doi.org/10.1016/S1876-3804(12)60011-1.
Zuo, M.S., Chen, H., Liu, X.L., et al., 2024. Fractal model of spontaneous imbibition in low-permeability reservoirs coupled with heterogeneity of pore seepage channels and threshold pressure. Pet. Sci. 21 (2), 1002–1017. https://doi.org/10.1016/j.petsci.2023.10.027.